# Polarization-controlled multifunctional polarization conversion in bilayer chiral metamaterials

**Weimeng Luan**
Shanghai University
**Yihao Zhang**
Shanghai University
**Xinzhuo Gao**
Shanghai University
**Xiaona Yan** ( xnyan@staff.shu.edu.cn )
Shanghai University
**Zuanming Jin**
Terahertz Technology Innovation Research Institute, University of Shanghai for Science and Technology
**Guohong Ma**
Shanghai University
**Jianquan Yao**
Tianjin University

**Research Article**

**Keywords:** Metamaterials, Chiral Terahertz, Polarization conversion, Multifunction

**Posted Date:** May 19th, 2022

**DOI:** https://doi.org/10.21203/rs.3.rs-1663679/v1

# Abstract

In this paper, a chiral metamaterial (MM) structure composed of bilayer twisted split-ring resonator (SRR) arrays is proposed and demonstrated to realize polarization-controlled, dual-directional, and multifunctional polarization conversion for terahertz (THz) waves. Simulated results show that the converter can selectively achieve linear-to-linear, or linear to left-handed circular, or linear to right-handed circular's polarization conversion according to the polarization state and propagating direction of the incident THz wave. Stokes parameters, ellipticity, and polarized rotation angle are introduced to determine the polarization states of the output waves. The circular polarization transmission coefficients and surface current distributions at the resonance frequency points are simulated to explain and demonstrate the physical origin of polarization conversion. The proposed multifunctional converter can find potential applications in THz sensing, imaging and communication areas.


# Introduction

Electromagnetic waves (EMWs) with controllable polarization state have shown excellent performance in the fields of antennas, communications, and sensing [1–3]. Polarization is one of the fundamental characteristics of EMWs. Polarization conversion is to transfer polarization state of the EMW to a predefined one, which is generally achieved by gratings, birefringent materials, and liquid crystals [4–6]. However, due to the inherent defects such as large size, low efficiency, and narrow bandwidth with these methods, their practical applications are severely limited.

MMs are artificially fabricated microstructural materials, which offer promising approaches for the control of polarization state [7, 8] because they enable abrupt changes to the amplitude [9, 10] and phase [10] of the scattered EMWs. Since Pendry predicted that a chiral route can be used to obtain negative refraction [11], the chirality concept in MMs has attracted significant attention. Chirality means that the structure cannot be brought into congruence with its mirror image unless lifted off the substrate. Thus, the optical response of the chiral MM is different for right-handed circularly polarized (RCP) and left-handed circularly polarized (LCP) incident waves [12]. It means that besides negative refraction, chiral MMs still possess optical activity [13, 14], circular dichroism [12, 15], and giant gyrotropy [16]. Accordingly, chiral MMs are of great interest for customized polarization state and have potential applications in polarization control devices, such as lens [17], polarization converter [18], and isolators [19]. So far, various chiral MMs based polarization converters have been proposed to obtain single-band [20, 21] or dual-band [22, 23] linear-to-linear polarization conversions, single-frequency [24] or dual-frequency [25, 26] linear-to-circular polarization conversion, etc. However, the above mentioned polarization converters can only achieve a single predefined polarization state. In some applications, such as smart radar and quantum communications [27, 28], we need that a specially designed chiral MM can realize multifunctional polarization conversion, that is, convert the incident polarization to two or more different output polarizations, such as linear, circular (RCP or LCP), or elliptical polarization. For example, based on circular dichroism and giant optical activity possessed in a double-layer twisted Y-shaped chiral MM structure, Ma et al. simultaneously realized linear-to-circular and linear-to-linear

polarization conversions at 12.28 GHz and 12.70 GHz, respectively [29]. Cheng et al. proposed an asymmetric chiral MM composed of bi-layer twisted split-ring structure to achieve circular polarized waves at 5.32 and 6.6 GHz, respectively, and cross-polarized wave at 10.52 GHz [30]. Actually, chiral MM based polarization converters are particularly attractive in THz frequency regime due to the lack of naturally responding THz materials. Till now, single-functional linear-to-linear [31, 32] or linear-to-circular [33, 34] THz polarization converters have been discussed a lot. However, reports on multifunctional polarization converters in THz regime are relatively few, in addition, most reported ones are based on dynamically modulated materials. For instance, by inserting temperature-controlled phase-change material vanadium dioxide ($VO_2$) into chiral MMs, Wu et al. [35] and Yan et al. [36] respectively proposed a switchable linear-to-linear and linear-to-circular polarization conversions in THz regime by adjusting the temperature. Obviously, to realize the switch from one type polarization conversion to another type, the adjustable parameter needs to be precisely controlled. However, due to the defects in manufacture, accordingly, the mismatch between simulation and experiment, it is not easy to determine this parameter accurately.

In this paper, we propose a polarization-controlled multifunctional polarization converter in THz regime. The converter is based on a chiral MM structure composed of bi-layered SRR arrays. Simulated results show that the polarization converter can switch from linear-to-linear to linear-to-circular polarization conversion by adjusting the polarization state of the normally incident wave. When a *y*-polarized wave incidents on the chiral MM along −z-axis, narrowband linear polarization conversion with the polarization conversion ratio (PCR) over 90% and bandwidth 0.15 THz is realized. However, for an incident *x*-polarized wave, linear-to-RCP and linear-to-LCP conversion with ellipticity $e \approx \pm 1$ occur at different frequency points. Moreover, the multifunctional polarization conversion is dual-directional.

## Structure Design, Theory And Simulation

# 1.1. Design and theory of multifunctional polarization conversion

Figure 1a, b show the schematic diagram of the proposed chiral MM structure and its working theory as a multifunctional polarization converter along two opposite propagating directions. The MM structure consists of bi-layered metallic SRR arrays separated by a polyimide dielectric layer. The schematic of one unit cell and its structural parameters are shown in Fig. 1c, in which the front SRR is rotated 90° clockwise with respect to the back one. To realize multifunctional polarization conversion, the optimized structural parameters are as follows: the outer and inner radii of the SRRs are $R = 35$ μm and $r = 25$ μm, respectively. Gap angle relative to the center of the SRR is $\theta = 20°$. The lattice constants of one unit cell along *x* and *y* axis are $P_x = P_y = 100$ μm. The flexible $t = 20$ μm thick polyimide film is treated as the dielectric spacer with dielectric constant $\varepsilon = 3.5$. All metallic SRRs are made of gold with conductivity $\sigma = 4.561 \times 10^7$ S/m and thickness 200 nm.

In order to study the polarization conversion property of the designed MM structure, we adopt full three-dimensional finite-difference time-domain solver of CST Microwave Studio for numerical simulations. Periodic boundary conditions are applied in the *x*- and *y*-directions, and the perfect match layer (PML) boundary conditions are imposed at the boundaries in *z*-direction. To ensure the accuracy, the length scale of the mesh is set to be less than or equal to $\lambda_0$ / 10 throughout the simulation domain, where $\lambda_0$ is the central wavelength of the incident THz radiation. In simulation, the THz waves are normally incident on the chiral MM structure.

Theories of the proposed MM structure for dual-directional and multifunctional polarization conversion is shown in Fig. 1a, b. For forward propagation (along -*z*-axis), a normally incident *x*-polarized wave is converted to transmitted LCP and RCP waves by the MM structure at resonant frequency points 0.49 THz and 0.59 THz, respectively; while a normally incident *y*-polarized wave along this propagating direction is converted to a transmitted *x*-polarized wave in a narrow-band with bandwidth 0.15 THz and central frequency 1.28 THz. On the other hand, for backward propagation (along + *z*-axis), due to chirality of the MM structure, a *y*-polarized incident wave is converted to RCP and LCP transmitted waves at 0.49 THz and 0.59 THz, respectively; while a *x*-polarized incident wave is converted to *y*-polarized transmitted wave at 1.28 THz. Therefore, by choosing appropriate polarization state and propagating direction of the incident wave, the MM structure can selectively realize linear-to-circular or linear-to-linear polarization conversion.

In the following, we will thoroughly characterize the polarization conversion performances of the chiral MM structure.

# 2.2 Linear-to-circular polarization conversion

In order to understand the linear-to-circular conversion performance of the chiral MM, we first simulate amplitude transmission spectra for co- and cross-polarized components and phase change between two orthogonally polarized components in the frequency range of 0.35 ~ 0.70 THz when incident *x*- and *y*-polarized waves respectively propagate along forward and backward directions, as shown in Fig. 2a, b, where the subscripts *m* and *n* represent *n*-polarized incident wave and *m*-polarized transmitted wave. Obviously, the transmission spectra for two co-polarized components coincide with each other, and so do two cross-polarized components, meanwhile, the phase changes along two propagation directions are equal in size but opposite in sign, indicating that the MM can realize dual-directional linear-to-circular polarization conversion. However, the handedness of the circular polarization along two opposite directions are contrary to each other because the phase difference is always defined as the phase of y-polarized component minus to that of x-polarized component of the transmitted waves. In the following, we will take the incident *x*-polarized wave propagating along the forward direction as an example to discuss the linear-to-circular polarization conversion performance.

Assuming electric field of the incident *x*-polarized wave is represented by $\vec{E}_i = E_{xi}\vec{e}_x$. After the MM structure, the electric field of the transmitted wave can be expressed as

$\vec{E}_t = E_{xi}(t_{xx}e^{j\varphi_{xx}}\vec{e}_x + t_{yx}e^{j\varphi_{yx}}\vec{e}_y)$, where $t_{xx}$, $t_{yx}$ and $\phi_{xx}$, $\phi_{yx}$ represent amplitudes and phases of transmission coefficients for *x*-to-*x* and *x*-to-*y* polarization conversion, respectively. It has been demonstrated that when two conditions, amplitudes $t_{xx} = t_{yx}$ and phase difference $\delta = \phi_{yx} - \phi_{xx} = 2n\pi \pm 0.5\pi$ are satisfied simultaneously, the perfect linear-to-circular polarization conversion can be achieved [37].

As shown in Fig. 2a-b, at resonant frequency points 0.49 THz and 0.59 THz, the transmission amplitudes $t_{yx}$ and $t_{xx}$ are almost the same and equal to 0.54 and 0.60, respectively. In addition, the phase differences $\delta$ are about 270° and 90°, respectively. Combining these results with the above mentioned conditions for linear-to-circular polarization conversion, it is proved that the transmitted waves are nearly perfect circular polarization. As the transmission amplitudes at two frequencies are larger than 0.5, the conversion efficiencies are high, indicating that the electromagnetic coupling between two metallic layers are strong.

To verify the above results and to characterize the handedness of the transmitted waves under *x*-polarization incidence, Stokes parameters are introduced [38, 39]:

$$\begin{aligned} S_0 &= t_{xx}^2 + t_{yx}^2, \\ S_1 &= t_{xx}^2 - t_{yx}^2, \\ S_2 &= 2t_{xx}t_{yx}\cos\delta, \\ S_3 &= 2t_{xx}t_{yx}\sin\delta. \end{aligned} \quad (1)$$

Correspondingly, the normalized ellipticity $e$ and elliptical angle $\chi$ are determined:

$$e = \frac{S_3}{S_0}, \quad \sin 2\chi = \frac{S_3}{S_0}. \quad (2)$$

where $e$ (or $\chi$) can be used to characterize the ellipticity and handedness of the transmitted CP waves. $e$ = -1 (or $\chi$ = -45°) and $e$ = + 1 (or $\chi$ = 45°) indicate that the transmitted waves are perfectly LCP wave and RCP wave, respectively [40].

Figure 2c and 2d depict the frequency responses of the ellipticity and elliptical angle for *x*-polarization incidence. In Fig. 2c, e is approximately equal to -1 at frequency 0.49 THz and + 1 at 0.59 THz, implying that the transmitted waves behave as LCP at 0.49 THz and RCP at 0.59 THz, respectively. Figure 2d further shows the elliptical angles $\chi$ at above two resonant frequency points, which are − 42.3° and 42.8°, respectively, close to ±45°. $e \approx \pm 1$ or $\chi \approx \pm 45°$ further demonstrate that the proposed chiral MM structure has an excellent linear-to-circular polarization conversion performance at two resonant frequency points 0.49 THz and 0.59 THz.

For *y*-polarization incidence along backward direction, due to the chirality of the proposed MM structure, the transmitted waves at 0.49 THz and 0.59 THz are RCP wave and LCP wave, respectively, the handedness of which are contrary to those along forward direction.

# 2.3 Linear-to-linear polarization conversion

To realize linear-to-linear polarization conversion, polarization state of the incident wave is *y*-polarization for forward direction, and *x*-polarization for backward direction, which are contrary to those in linear-to-circular polarization conversion. Figure 3a shows the amplitude transmission spectra for cross- and co-polarized components when *y*- and *x*-polarized wave incident from two opposite directions. Obviously, two co-polarized components coincide with each other, so do two cross-polarized components. It means that the designed MM structure can also realize dual-directional linear-to-linear polarization conversion, and the conversion performances along two opposite directions are exactly the same. Taking the incident *y*-polarized wave along forward direction as an example, we discuss the performance of linear-to-linear polarization conversion.

Assuming electric fields of the incident wave and transmitted wave are $\vec{E}_i = E_{yi}\vec{e}_y$ and $\vec{E}_t = E_{yj}(t_{yy}e^{j\varphi_{yy}}\vec{e}_y + t_{xy}e^{j\varphi_{xy}}\vec{e}_x)$, respectively, where $t_{yy}$, $t_{xy}$ and $\phi_{yy}$, $\phi_{xy}$ are amplitudes and phases of the transmission coefficients for *y*-to-*y* and *y*-to-*x* polarization conversion, respectively. The performance of the linear-to-linear polarization conversion is often evaluated by PCR and polarization rotation angle $\psi$. The PCR is defined as [39, 41]:

$$PCR = \frac{t_{xy}^2}{t_{yy}^2 + t_{xy}^2}. \quad (3)$$

Introducing the similar Stokes parameters as Eq. 1, the polarization rotation angle $\psi$ is acquired [39]:

$$tg2\psi = \frac{S_2}{S_1} \quad (4)$$

As illustrated in Fig. 3a, at resonant frequency 1.28 THz, the designed MM structure exhibits quite different transmissions for the cross- and co-polarizations. The transmission of cross-polarization is nearly up to 0.80, while that of the co-polarization is less than 0.10. The remarkable difference in transmissions between two orthogonally polarized components suggests that the MM structure can realize linear-to-linear polarization conversion, that is, the incident *y*-polarized wave is converted to transmitted *x*-polarized wave for forward direction and the incident *x*-polarized wave is converted to transmitted *y*-polarized wave for backward direction. Figure 3b shows the frequency responses of PCR and polarization rotation angle $\psi$. It is found that in the range of 1.22~1.37 THz, the PCR is close to 90% and $\psi$ reaches + 90° or -90°, revealing that an incident linearly polarized wave transmitting through the

MM structure can perfectly convert to its cross-polarized direction. In addition, the linear-to-linear polarization conversion can occur at a narrow-band with bandwidth 0.15 THz and central frequency 1.28 THz.

Based on former discussions, we can conclude that the proposed chiral MM structure can not only realize dual-directional linear-to-circular polarization conversion, but also realize dual-directional linear-to-linear polarization conversion. The polarization states of the output waves depend on propagating direction and polarization state of the incident waves.

## 2.4 Electric field vector evolution in polarization conversion

To visually elucidate the polarization conversion process of the proposed MM structure, we simulate the evolutions of electric field in the *y*–*z* plane at polarization conversion frequency points 0.49 THz, 0.59 THz, and 1.28 THz, shown as Fig. 4. In Fig. 4a and b, when an *x*-polarized wave (the electric field is along −*x*-axis) transmits through the MM structure along forward direction, electric field vectors of the transmitted waves gradually rotate clockwise to right upper and counterclockwise to right down, respectively. Obviously, the output waves are LCP and RCP waves, as the electric fields satisfy left-handed and right-handed helix properties at frequencies 0.49 THz and 0.59 THz, respectively. In Fig. 4c, at 1.28 THz, when a *y*-polarized wave transmits through the MM structure along forward direction, the electric field vector of the transmitted wave is converted to + *x*-axis direction and linear-to-linear polarization conversion realizes. Obviously, electric field evolutions of the output waves are consistent well with elliptical angle and polarization rotation angle in Fig. 2 and Fig. 3.

## Discussions

To understand the physical origin of linear-to-circular polarization conversions at resonant frequency points 0.49 THz and 0.59 THz, we simulate the circular polarization transmission coefficients and surface current distributions at two frequency points, shown as Fig. 5. For an incident *x*-polarized wave, the circular polarization transmission coefficients $|C_+|$ (RCP) and $|C_-|$ (LCP) of the MM structure are defined as: $C_{\pm} = t_{xx}e^{j\varphi_{xx}} \pm jt_{yx}e^{j\varphi_{xy}}$ [42], numerical results for which are presented in Fig. 5a. It can be seen that at frequency points 0.49 THz and 0.59 THz, the minimum transmission coefficients for LCP and RCP waves are about 0.046 and 0.048, respectively. Meanwhile, the maximum transmission coefficients are up to 0.75 and 0.79, respectively. It indicates that one of the circular polarizations is almost eliminated at a specific resonant frequency, while the other is transmitted with a small loss. Thus, at 0.49 THz, the transmitted wave is LCP wave; at 0.59 THz, the RCP wave is transmitted. It proves that the linear-to-circular polarization conversion in chiral MM structure originates from the different circular polarization transmission coefficients for the LCP and RCP components at resonant frequencies[42].

In order to understand the nature of the resonances occurring at 0.49 and 0.59 THz, Fig. 5b simulates the surface current distributions at two resonant frequency points for *x*-polarization incidence, in which the real and dotted arrows represent the instantaneous current flows on the front and back SRRs in one unit cell, respectively. It is seen that at 0.49 THz, the surface currents on the twisted SRR pairs are in parallel,

while at 0.59 THz, the surface currents are anti-parallel. The surface current distribution or resonant modes at these two frequency points can be explained by hybridized coupling. For the 90° twisted SRR pairs MM, the back SRR is directly excited by the incident wave due to its orientation with respect to the incident electric field, then by near-field coupling between two SRRs the front SRR is excited. Hybridization coupling between two excited SRRs can lead to the formation of two new plasmonic modes, the symmetric mode and antisymmetric mode at 0.49 and 0.59 THz, respectively. As the electric fields in the slit gaps of two SRRs are perpendicular to one another, the electric dipole-dipole interaction equals zero. As a consequence, the new plasmonic modes are determined by the longitudinal magnetic dipole-dipole coupling [42, 43]. At 0.49 THz, the surface currents on the twisted SRR pairs are in parallel, leading to parallel magnetic dipole moments for the twisted SRR pairs. In contrast, at 0.59 THz, the surface currents on the twisted SRR pairs are anti-parallel, which results in antiparallel magnetic dipole moments. The two different magnetic dipole moments excited at 0.49 THz and 0.59 THz correspond to linear to LCP and linear to RCP conversion, respectively. Thus, from the surface current distribution, we can conclude that the reason for the transmitted RCP and LCP wave is the hybridization coupling between magnetic dipoles induced on two twisted SRRs.

To understand the linear-to-linear polarization conversion, we simulate the distributions of surface current and induced magnetic field for a *y*-polarized incident wave propagating along forward direction at resonant frequency 1.28 THz, shown as Fig. 6a. It can be seen that the front SRR generates higher-order resonant mode, while the back SRR corresponds to dipole resonant mode. The antiparallel currents between the front and back layers excite three current loops and result in magnetic dipole moments $m_1$- $m_3$. Each magnetic dipole moment contributes a magnetic field that can be decomposed into two components, parallel and perpendicular to the incident electric field $E_{in}$, among which $H_{y1}$- $H_{y3}$ are along the *y* axis and are parallel to the incident electric field $E_{in}$, while $H_{x1}$- $H_{x3}$ are along the *x* axis and are perpendicular to $E_{in}$, depicted in Fig. 6b. The cross coupling between $E_{in}$ and parallel magnetic field $H_{y1}$- $H_{y3}$ leads to polarization rotation, which causes the incident *y*-polarized wave convert to the *x*-polarized wave. On the other hand, no cross coupling exits between $E_{in}$ and perpendicular magnetic fields, which means $H_{x1}$- $H_{x3}$ make no contribution to polarization conversion. Thus, the cross-coupling between the incident electric field and induced magnetic field is the physical origin of linear-to-linear polarization conversion [44] .

In addition, the effects of oblique incidence on the polarization conversion performance are investigated. Simulated results show that the linear-to-circular polarization converter can only work at normal incidence due to the phase difference between two polarized components at resonance frequency is very sensitive to incident angle (not show here), while the linear-to-linear polarization conversion is robust to the incident angle. Figure 7 plots PCRs of the linear-to-linear polarization conversion as a function of incident angle and frequency. As incident angle varies from 0° to 60°, the PCR keeps at a higher and constant value, while the conversion bandwidth for *y*-polarized incident wave is broadened and the bandwidth for *x*-polarized incident wave is narrowed, shown as Fig. 7a and b, respectively. However, in the range of 0° to 30°, the linear-to-linear polarization converter is insensitive to the incident angle.

# Conclusion

In conclusion, we designed a chiral MM composed of two twisted SRR array layers for realizing dual-directional and multifunctional polarization conversion in THz regime. Along forward (backward) direction, the incident *x*(*y*)-polarized THz wave is converted to transmitted LCP (RCP) and RCP (LCP) waves at resonant frequency points 0.49 THz and 0.59 THz, respectively, while the incident *y(x)*-polarized wave is converted to *x(y)*-polarized wave in the frequency range of 1.22–1.37 THz with central frequency 1.28 THz. By analyzing the surface current distributions, we conclude that linear-to-circular polarization conversion originates from hybrid coupling between two magnetic dipoles, which results in different circular polarization transmission coefficients for LCP and RCP waves; and the linear-to-linear polarization conversion originates from the cross coupling between the incident electric field and induced magnetic field. The designed MM structure can be utilized as a dual-directional, multifunctional, and polarization-controlled circular and linear polarization converter in THz imaging, sensing, and communications.

# Declarations


### Funding Information

This work was supported by the National Natural Science Foundation of China (NSFC, Nos. 92150101, 61735010)


**Authors' contribution** All authors contributed to the study conception and design. CST calculations and data collection and analysis were done by Weimeng Luan, Yihao Zhang, Xiaona Yan, Xinzhuo Gao, Guohong Ma, Jianquan Yao; Manuscript paper was written by Weimeng Luan, and revised by Zuanming Jin. All authors have read and agreed to the published version of the manuscript.

**Availability of Data and Material** The datasets generated during and/or analyzed during the current study are available from the corresponding author on reasonable request.

**Code Availability** The codes used during the current study are available from the corresponding author on reasonable request.

**Ethics approval** We have followed the ethical principles and accurate references to scientific sources in our original article. This research does NOT involve human participants or animal; thus, no ethical approval and patient consent are required.

**Consent to participate** The authors consent to participate.

**Consent for Publication** The authors consent to publish.

**Conflict of Interest** The authors declare no competing interests.

# References


1. Xu H-X, Wang G-M, Qi M-Q (2013) A miniaturized triple-band metamaterial antenna with radiation pattern selectivity and polarization diversity. PIER 137:275–292. https://doi.org/10.2528/PIER12081008
2. Wang Y, Yang C, Wang Y, et al (2014) Gigabit polarization division multiplexing in visible light communication. Opt Lett 39:1823. https://doi.org/10.1364/OL.39.001823
3. Barreda ÁI, Sanz JM, González F (2015) Using linear polarization for sensing and sizing dielectric nanoparticles. Opt Express 23:9157. https://doi.org/10.1364/OE.23.009157
4. Yamada I, Takano K, Hangyo M, et al (2009) Terahertz wire-grid polarizers with micrometer-pitch Al gratings. Opt Lett 34:274. https://doi.org/10.1364/OL.34.000274
5. Cerjan A, Fan S (2017) Achieving Arbitrary Control over Pairs of Polarization States Using Complex Birefringent Metamaterials. Phys Rev Lett 118:253902. https://doi.org/10.1103/PhysRevLett.118.253902
6. Wiesauer K, Jördens C (2013) Recent Advances in Birefringence Studies at THz Frequencies. J Infrared Milli Terahz Waves 34:663–681. https://doi.org/10.1007/s10762-013-9976-4
7. Zárate Y, Babaee S, Kang SH, et al (2016) Elastic metamaterials for tuning circular polarization of electromagnetic waves. Sci Rep 6:28273. https://doi.org/10.1038/srep28273
8. Zeng F, Ye L, Li L, et al (2019) Tunable mid-infrared dual-band and broadband cross-polarization converters based on U-shaped graphene metamaterials. Opt Express 27:33826. https://doi.org/10.1364/OE.27.033826
9. Su X, Xu Q, Ouyang C, et al (2015) Switchable terahertz metamaterials in resonance amplitude. In: 2015 40th International Conference on Infrared, Millimeter, and Terahertz waves (IRMMW-THz). IEEE, Hong Kong, China, pp 1–2
10. Cojocari MV, Schegoleva KI, Basharin AA (2017) Blueshift and phase tunability in planar THz metamaterials: the role of losses and toroidal dipole contribution. Opt Lett 42:1700. https://doi.org/10.1364/OL.42.001700
11. Pendry JB (2004) A Chiral Route to Negative Refraction. Science 306:1353–1355. https://doi.org/10.1126/science.1104467
12. Decker M, Klein MW, Wegener M, et al (2007) Circular dichroism of planar chiral magnetic metamaterials. Opt Lett 32:856. https://doi.org/10.1364/OL.32.000856
13. Decker M, Zhao R, Soukoulis CM, et al (2010) Twisted split-ring-resonator photonic metamaterial with huge optical activity. Opt Lett 35:1593. https://doi.org/10.1364/OL.35.001593
14. Ren M, Plum E, Xu J, et al (2012) Giant nonlinear optical activity in a plasmonic metamaterial. Nat Commun 3:833. https://doi.org/10.1038/ncomms1805
15. Kwon D-H, Werner PL, Werner DH (2008) Optical planar chiral metamaterial designs for strong circular dichroism and polarization rotation. Opt Express 16:11802. https://doi.org/10.1364/OE.16.011802

16. Rogacheva AV, Fedotov VA, Schwanecke AS, et al (2006) Giant Gyrotropy due to Electromagnetic-Field Coupling in a Bilayered Chiral Structure. Phys Rev Lett 97:177401. https://doi.org/10.1103/PhysRevLett.97.177401
17. Shevchenko VV (2009) The geometric-optics theory of a plane chiral-metamaterial lens. J Commun Technol Electron 54:662–666. https://doi.org/10.1134/S1064226909060060
18. Fan R-H, Zhou Y, Ren X-P, et al (2015) Freely Tunable Broadband Polarization Rotator for Terahertz Waves. Adv Mater 27:1201–1206. https://doi.org/10.1002/adma.201404981
19. Wang L, Huang X, Li M, et al (2019) Chirality selective metamaterial absorber with dual bands. Opt Express 27:25983. https://doi.org/10.1364/OE.27.025983
20. Tian Y, Chen Z, Ren F-F, et al (2021) High-Efficiency Asymmetric Transmission of Red-Near-Infrared Light Based on Chiral Metamaterial. Front Phys 9:676840. https://doi.org/10.3389/fphy.2021.676840
21. Wang L, Lv F, Xiao Z, et al (2021) Theoretical and Experimental Verification of 90° Polarization Converter Based on Chiral Metamaterials. Plasmonics 16:199–204. https://doi.org/10.1007/s11468-020-01278-5
22. Li ML, Zhang Q, Qin FF, et al (2017) Microwave linear polarization rotator in a bilayered chiral metasurface based on strong asymmetric transmission. J Opt 19:075101. https://doi.org/10.1088/2040-8986/aa72fd
23. Liu W, Wu W, Huang L, et al (2019) Dual-band asymmetric optical transmission of both linearly and circularly polarized waves using bilayer coupled complementary chiral metasurface. Opt Express 27:33399. https://doi.org/10.1364/OE.27.033399
24. Han D, Fang X, Zhang L, et al (2021) Tunable chiral responses in mechanically reconfigurable three-dimensional metamaterials. New J Phys 23:053001. https://doi.org/10.1088/1367-2630/abf86f
25. Cao H, Wu X, Pi Y, et al (2016) A novel chiral metamaterial circular polarizer based on e-shape structure. In: 2016 IEEE International Symposium on Antennas and Propagation (APSURSI). IEEE, Fajardo, PR, USA, pp 489–490
26. Cheng ZZ, Cheng YZ, Fang C (2014) Compact asymmetric metamaterial circular polarization transformer based on twisted double split-ring resonator structure. Journal of Electromagnetic Waves and Applications 28:485–493. https://doi.org/10.1080/09205071.2013.875861
27. Heilmann R, Gräfe M, Nolte S, et al (2015) Arbitrary photonic wave plate operations on chip: Realizing Hadamard, Pauli-X and rotation gates for polarisation qubits. Sci Rep 4:4118. https://doi.org/10.1038/srep04118
28. Chambers B (1999) A smart radar absorber. Smart Mater Struct 8:64–72. https://doi.org/10.1088/0964-1726/8/1/007
29. Ma X, Huang C, Pu M, et al (2013) Circular Dichroism and Optical Rotation in Twisted Y-Shaped Chiral Metamaterial. Appl Phys Express 6:022001. https://doi.org/10.7567/APEX.6.022001
30. Cheng Y, Nie Y, Cheng Z, et al (2014) DUAL-BAND CIRCULAR POLARIZER AND LINEAR POLARIZATION TRANSFORMER BASED ON TWISTED SPLIT-RING STRUCTURE ASYMMETRIC

CHIRAL METAMATERIAL. PIER 145:263–272. https://doi.org/10.2528/PIER14020501

31. Fang S, Luan K, Ma HF, et al (2017) Asymmetric transmission of linearly polarized waves in terahertz chiral metamaterials. Journal of Applied Physics 121:033103. https://doi.org/10.1063/1.4974477
32. Liu D, Xiao Z, Ma X, et al (2016) Broadband asymmetric transmission and polarization conversion of a linearly polarized wave based on chiral metamaterial in terahertz region. Wave Motion 66:1–9. https://doi.org/10.1016/j.wavemoti.2016.05.003
33. Masyukov M, Vozianova A, Grebenchukov A, et al (2020) Optically tunable terahertz chiral metasurface based on multi-layered graphene. Sci Rep 10:3157. https://doi.org/10.1038/s41598-020-60097-0
34. Dong X, Liu C, Huang Y, et al (2020) Angular-dependent circular dichroism of Tai Chi chiral metamaterials in terahertz region. Appl Opt 59:3686. https://doi.org/10.1364/AO.387150
35. Wu X, Lan F, Shi Z, et al (2017) Switchable terahertz polarization conversion via phase-change metasurface. In: 2017 Progress In Electromagnetics Research Symposium - Spring (PIERS). IEEE, St. Petersburg, pp 102–106
36. Yan D-X, Feng Q-Y, Yuan Z-W, et al (2022) Wideband switchable dual-functional terahertz polarization converter based on vanadium dioxide-assisted metasurface. Chinese Phys B 31:014211. https://doi.org/10.1088/1674-1056/ac05a7
37. Quader S, Zhang J, Akram MR, et al (2020) Graphene-Based High-Efficiency Broadband Tunable Linear-to-Circular Polarization Converter for Terahertz Waves. IEEE J Select Topics Quantum Electron 26:1–8. https://doi.org/10.1109/JSTQE.2020.2969566
38. Cong L, Cao W, Zhang X, et al (2013) A perfect metamaterial polarization rotator. Appl Phys Lett 103:171107. https://doi.org/10.1063/1.4826536
39. Cong L, Cao W, Tian Z, et al (2012) Manipulating polarization states of terahertz radiation using metamaterials. New J Phys 14:115013. https://doi.org/10.1088/1367-2630/14/11/115013
40. Guan S, Cheng J, Chen T, et al (2020) Widely tunable polarization conversion in low-doped graphene-dielectric metasurfaces based on phase compensation. Opt Lett 45:1742. https://doi.org/10.1364/OL.385159
41. Wu PC, Zhu W, Shen ZX, et al (2017) Broadband Wide-Angle Multifunctional Polarization Converter via Liquid-Metal-Based Metasurface. Advanced Opt. Mater 5:1600938. https://doi.org/10.1002/adom.201600938
42. Mutlu M, Akosman AE, Serebryannikov AE, et al (2011) Asymmetric chiral metamaterial circular polarizer based on four U-shaped split ring resonators. Opt Lett 36:1653. https://doi.org/10.1364/OL.36.001653
43. Liu N, Liu H, Zhu S, et al (2008) Stereometamaterials. Nature Photon 3:157. https://doi.org/10.1038/nphoton.2009.4
44. Zhang P, Zhao M, Wu L, et al (2013) Giant circular polarization conversion in layer-by-layer nonchiral metamaterial. J Opt Soc Am A 30:1714. https://doi.org/10.1364/JOSAA.30.001714

# Figures

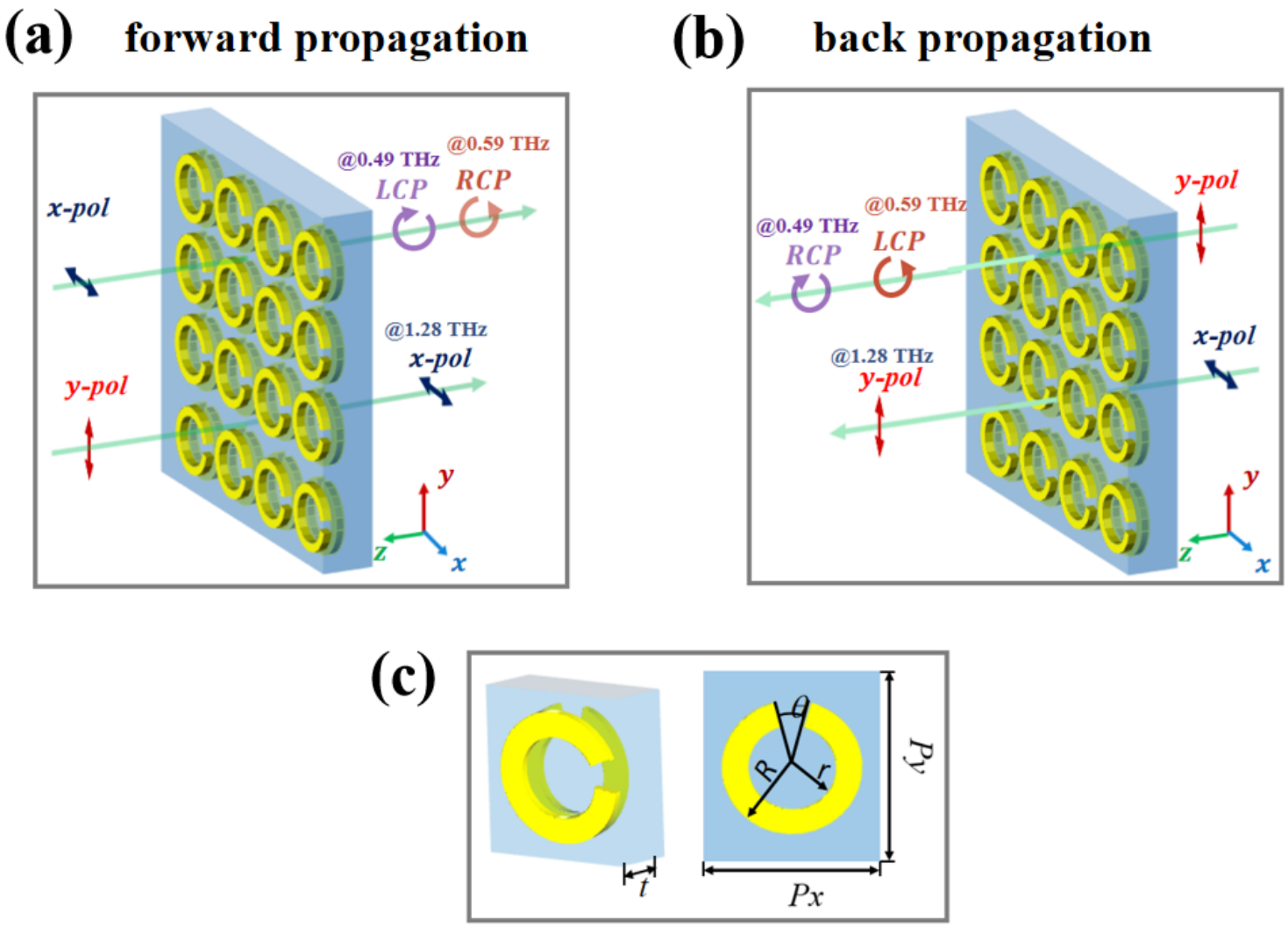


**Figure 1**

**a, b** The proposed chiral MM structure and its polarization conversion theories along two opposite propagating directions; **c** One unit cell and its structural parameters: $R$ = 34 mm, $r$ = 20 mm, θ = 20°, $t$ = 20 mm, $P_x$ = $P_y$ = 100 μm.

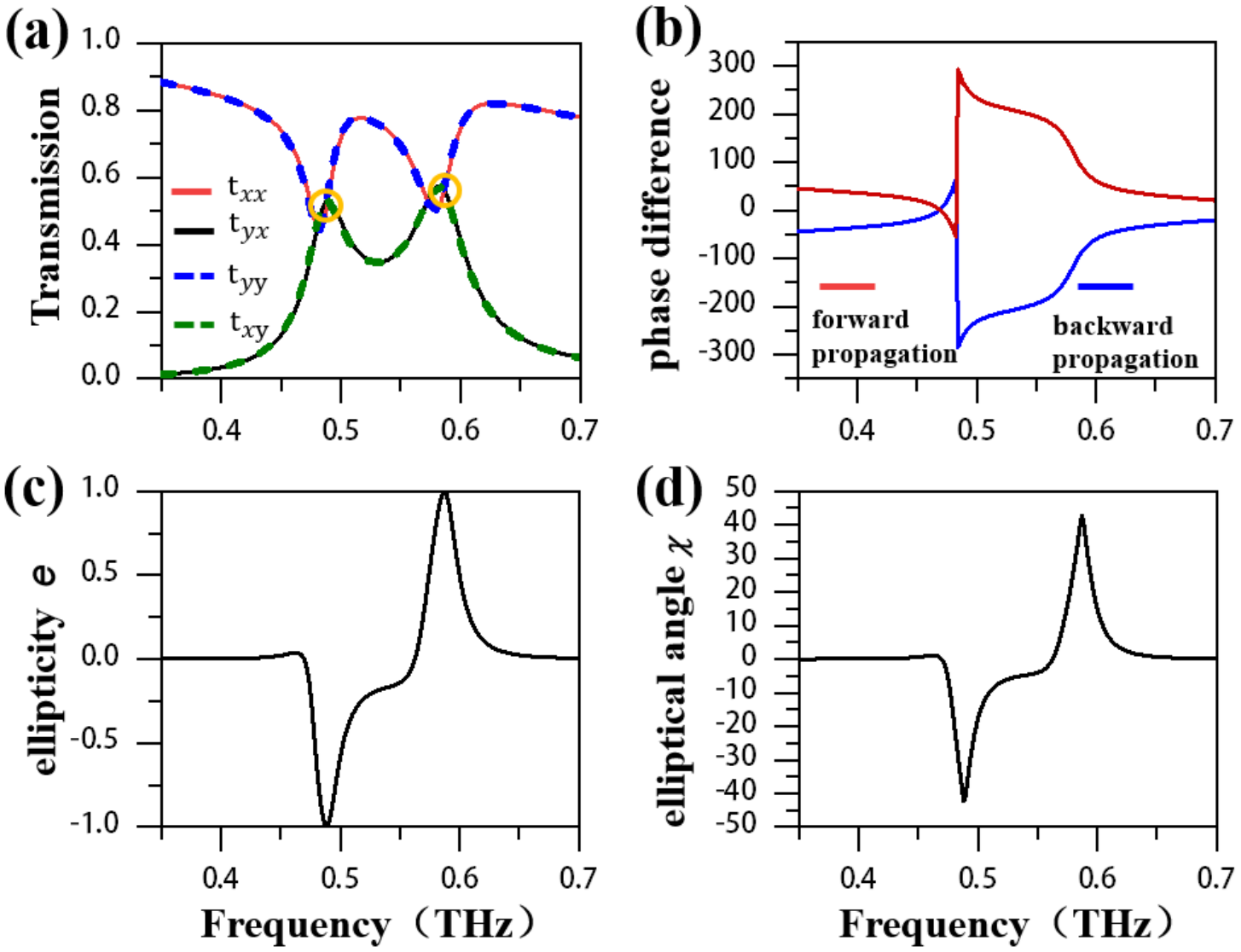


**Figure 2**

Simulated results for linear-to-circular polarization conversion. **a** Amplitude transmission spectra for cross- and co-polarized components when *x*-polarized wave propagates along forward direction and *y*-polarized wave propagates along backward direction, respectively; **b** Phase difference (in degree) between *y*- and *x*-polarized components along two propagating directions; The frequency responses of **c** ellipticity *e,* and **d** elliptical angle c (in degree) for *x*-polarization incidence along forward direction.

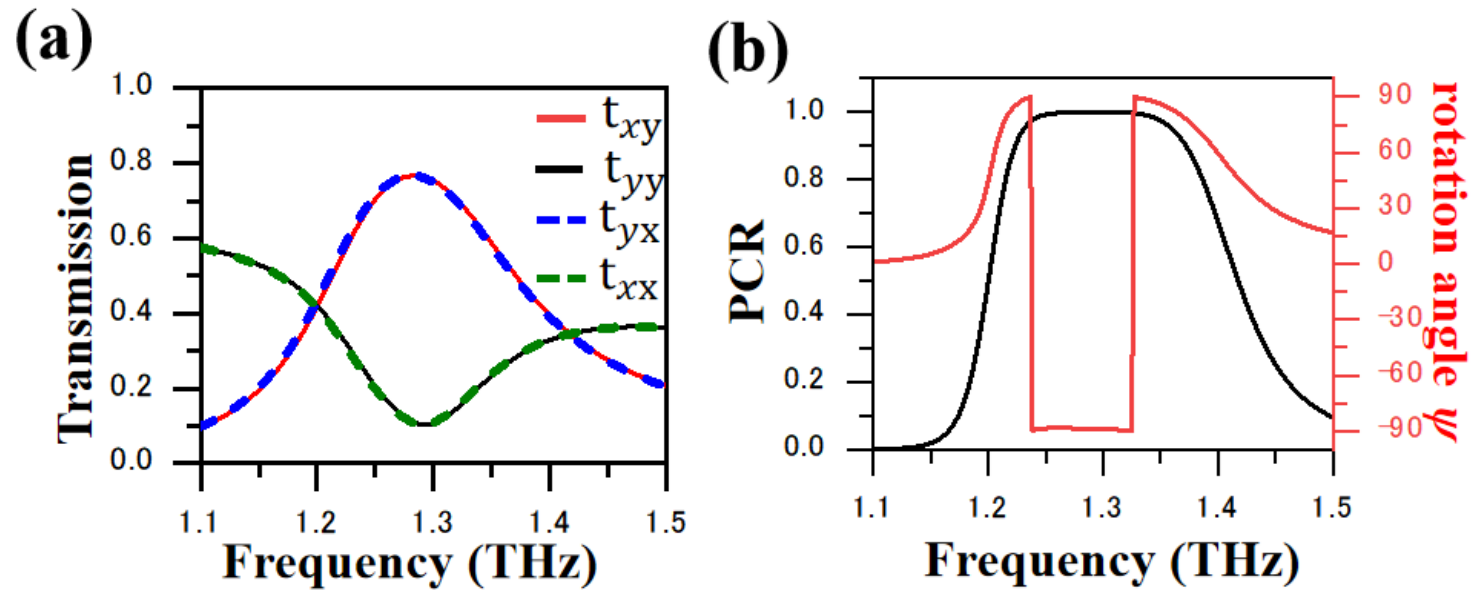


Figure 3

Simulated results for linear-to-linear polarization conversion. **a** Amplitude transmission spectra for cross- and co-polarized components when *y*-polarized wave propagates along forward direction and *x*-polarized wave propagates along backward direction, respectively; **b** The PCR and polarization rotation angle Ψ (in degree) for *y*-polarized wave propagating along forward direction.

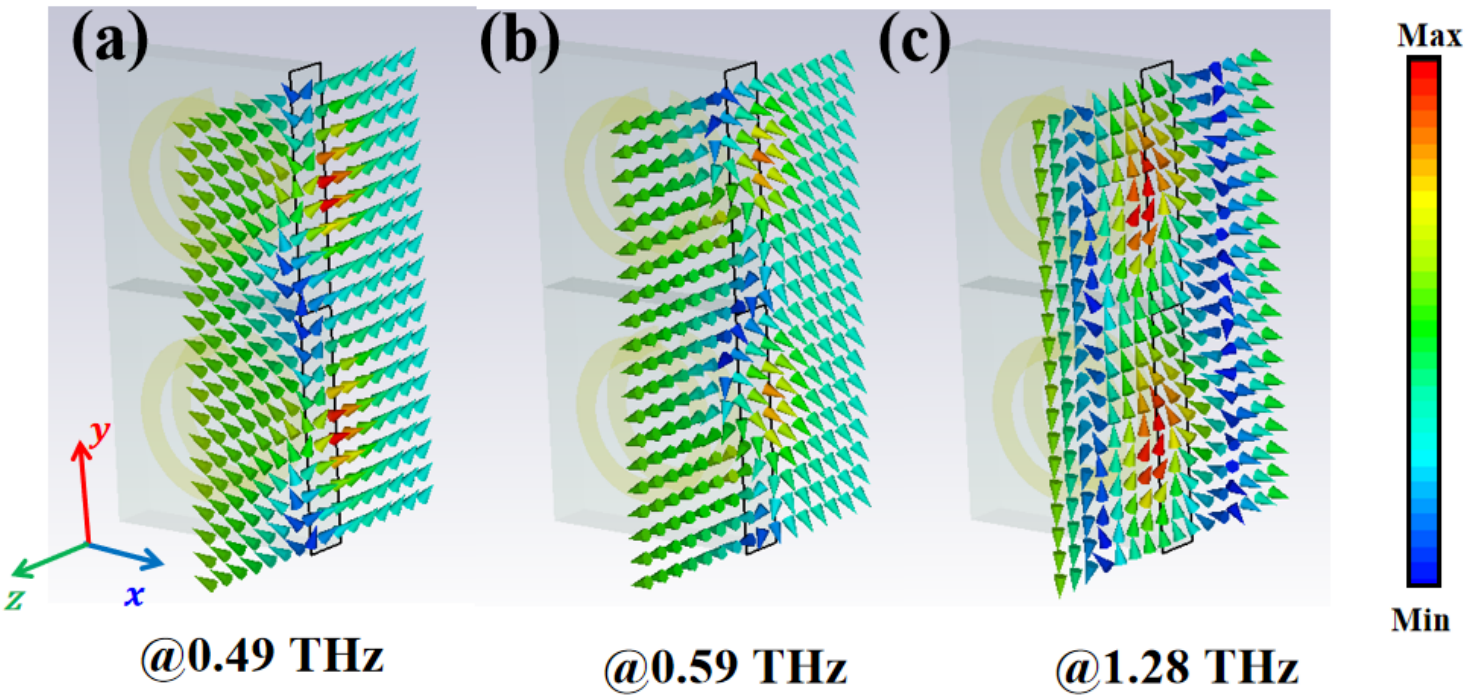


Figure 4

Evolutions of the electric field vector at three resonant frequency points.

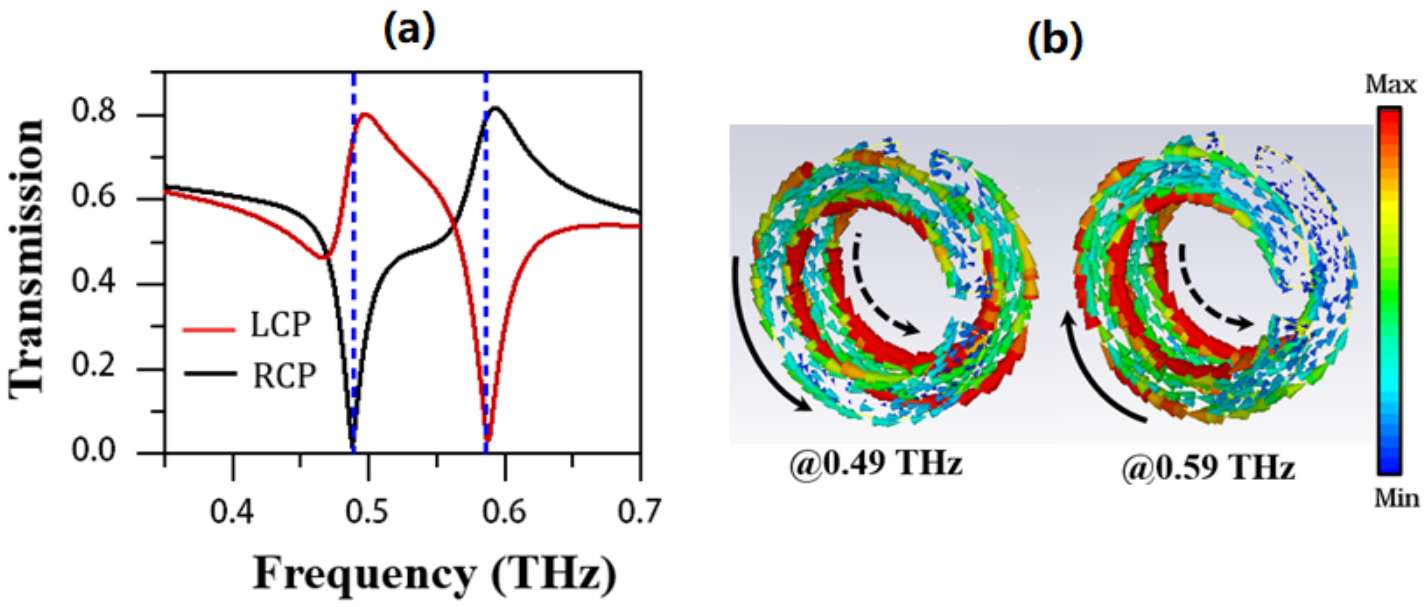


Figure 5

**a** Numerical results for the circular polarization transmission coefficients of the chiral MM; **b** Surface current distributions of one unit cell on two resonant frequency points.

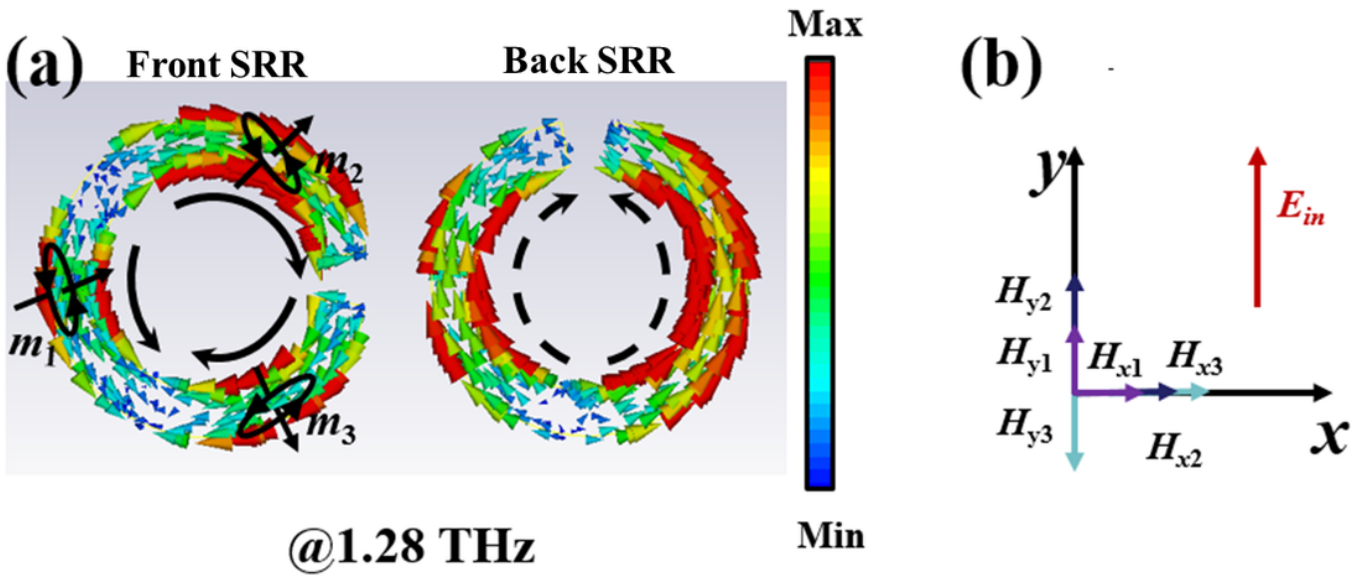


Figure 6

**a** The surface current distributions for two SRRs in one unit cell and the induced magnetic dipole moments between two layers at resonant frequency 1.28 THz, **b** decomposition of the induced magnetic fields on *x*- and *y*-axis.

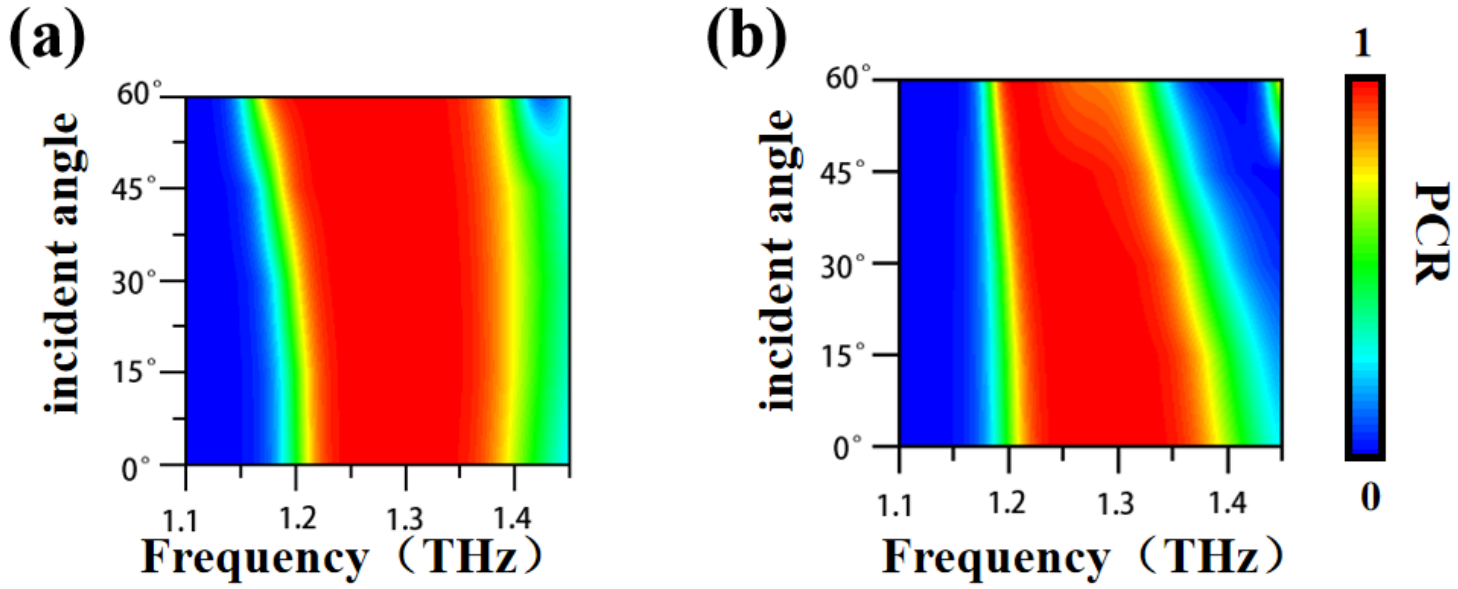


## Figure 7

In linear-to-linear polarization conversion, the frequency response of PCR with respect to incident angles for **a** *y*-polarized incident wave along forward direction and **b** *x*-polarized incident wave along backward direction, respectively.